



Dynamic Mechanisms Associated with the Structure and Evolution of Roll Vortices and Coherent Turbulence in the Hurricane Boundary Layer: A Large Eddy Simulation During the Landfall of Hurricane Harvey

Xin Li¹ · Zhaoxia Pu¹

Received: 27 October 2022 / Accepted: 2 December 2022 / Published online: 4 January 2023
© The Author(s) 2022

Abstract

Roll vortices are a series of large-scale turbulent eddies that nearly align with the mean wind direction and prevail in the hurricane boundary layer. In this study, the one-way nested WRF-LES model simulation results from Li et al. (J Atmos Sci 78(6):1847–1867, <https://doi.org/10.1175/JAS-D-20-0270.1>, 2021) are used to examine the structure and generation mechanism of roll vortices and associated coherent turbulence in the hurricane boundary layer during the landfall of Hurricane Harvey from 00 UTC 25 to 18 UTC 27 August 2017. Results indicate that roll vortices prevail in the hurricane boundary layer. The intense roll vortices and associated large turbulent eddies above them (at a height of ~ 200 to 3000 m) accumulate within a hurricane radius of 20–40 km. Their intensity is proportional to hurricane intensity during the simulation period. Before and during hurricane landfall, strong inflow convergence leads to horizontal advection of roll vortices throughout the entire hurricane boundary layer. Combined with the strong wind shear, the strongest roll vortices and associated large turbulent eddies are generated near the eyewall with suitable thermodynamic (Richardson number at around -0.2 to 0.2) and dynamic conditions (strong negative inflow wind shear). After landfall, the decayed inflow weakens the inflow convergence and quickly reduces the strong roll vortices and associated large turbulent eddies. Diagnosis of vertical turbulent kinetic energy indicates that atmospheric pressure perturbation, caused by horizontal convergence, transfers the horizontal component of turbulence to the vertical component with a mean wavelength of about 1 km. The buoyancy term is weak and negative, and the large turbulent eddies are suppressed.

Keywords Roll vortices · Coherent turbulence · Hurricane boundary layer · Inflow convergence · Pressure perturbation · Large eddy simulation

✉ Zhaoxia Pu
Zhaoxia.Pu@utah.edu

¹ Department of Atmospheric Sciences, University of Utah, Salt Lake City, USA

1 Introduction

Roll vortices are a series of large-scale turbulent eddies (Etling and Brown 1993; Mourad and Walter 1996; Weckwerth et al. 1997; Young et al. 2002). They can be resident in the hurricane boundary layer (Wurman and Winslow 1998; Katsaros et al. 2000, 2002; Huang et al. 2018). They can also enhance momentum, energy, and composition exchange in the atmospheric boundary layer (Fujita 1992; Kepert 1996; Makin 1998; Lorsolo et al. 2008; Zhang et al. 2008; Ellis and Businger 2010; Gao et al. 2017). Improved understanding of the mechanism of roll vortices can enhance comprehension of the planetary boundary layer (PBL) and consequently atmospheric predictions, especially for intensely damaging hurricanes (Ernst et al. 2019).

Previous studies have found that roll vortices in the hurricane boundary layer can nearly align with or be significantly different from the mean wind, with wavelength varying from 200 m to over 3000 m (Gall et al. 1998; Wurman and Winslow 1998; Lorsolo et al. 2008; Morrison et al. 2005; Nolan 2005). Morrison et al. (2005) verified from radar observations that roll vortices are oriented approximately 4° to the left of the mean wind and extend from 200 to 800 m above the ground in the hurricane boundary layer. Through radar and satellite observations, Huang et al. (2018) found that the wavelength of a roll in the marine atmospheric boundary layer is shortest near the storm centre and increases and then decreases with distance from the storm centre. Moreover, compared to numerical flux simulations with the PBL scheme in mesoscale models (e.g., Hong and Pan 1996; Hong et al. 2006; Hong 2010), some of the fluxes associated with roll vortices can be about 2–3 times greater (Morrison et al. 2005; Zhu 2008b; Gao and Ginis 2016). Strong fluxes induced by roll vortices change the hurricane structure and finally impact hurricane damage through intense surface winds (Saffir 1973; Wakimoto and Black 1994).

While many previous studies have emphasized the structure of roll vortices and their influence on hurricane structure and evolution, the dynamic mechanism that causes the genesis of hurricane roll vortices has remained under continuing investigation. LeMone (1973) found that rolls in the PBL are maintained primarily by the energy of the buoyancy and/or smaller turbulent eddies that reinforce the rolls. A theoretical study (Foster 2005) and several idealized numerical simulations (Gao and Ginis 2014) have found that hurricane roll vortices are caused by inflow inflection point instability, namely dynamic instability near the height with the sharpest inflow change of the profiles, similar to roll vortices in the Ekman layer (Lilly 1966; Brown 1980). Young et al. (2002) found that the different instability of wind components can lead to a different kind of roll. Foster (2005) used a theoretical study of roll vortices to verify that aligned with the mean wind, roll vortices are dominated by the inflection point of radial wind. Moreover, in the hurricane boundary layer, the dynamic instability with wind shear generates a quasi-equilibrium roll near neutral conditions, once the divergence of the roll fluxes transfers kinetic and/or potential energy from the perturbation back into the mean flow at the same rate at which it is extracted (LeMone 1973; Brown 1980). Specifically, strong buoyancy forcing inhibits the rolls, and they can be generated only when the flux Richardson number (R_f) is less than 0.25. With an idealized simulation, Gao and Ginis (2014) further confirmed that the rate of generation of roll vortices (w') is positively correlated with the strength of the inflow shear there. However, their finding has not yet been confirmed with a real hurricane due to the lack of high-resolution observations.

Fortunately, numerical simulations can provide insights into the structure of roll vortices inside a hurricane (Nakanishi and Niino 2012; Gao and Ginis 2014, 2016, 2018). Large eddy

simulation (LES), which is commonly used to simulate turbulence in the atmospheric boundary layer, can also be used to simulate roll vortices in the hurricane boundary layer (Nakanishi and Niino 2012; Wang and Jiang 2017). Since LES was introduced into the Weather Research and Forecasting Model (WRF) (Skamarock et al. 2019), large turbulent eddies, including roll vortices, have been simulated in real hurricanes by LES through nested grids within an advanced research version of the community Weather Research and Forecasting (WRF-LES) model (Zhu 2008a; Zhu et al. 2016). With LES, the strong fluxes associated with large eddies can be simulated without using a PBL parameterization scheme (Zhu 2008b). In a recent study, Li et al. (2021) used the WRF-LES model to simulate Hurricane Harvey (2017) around its landfall and analyzed the impact of large turbulent eddies on the evolution of the hurricane before, during, and after landfall. They found that roll vortices were reasonably simulated by WRF-LES. Their diagnoses also found that large turbulent eddies, including roll vortices, could generate a strong flux near the hurricane eyewall and influence the wind structure and precipitation of the hurricane during its landfall.

Following Li et al. (2021), in this study we further *evaluate the dynamic mechanisms associated with the structure and evolution of roll vortices and other large turbulent eddies in the hurricane boundary layer, with the goal of enhancing understanding of mechanisms that lead to the generation and decay of large eddies in a real hurricane*. The WRF-LES model setup and turbulence data processing are briefly described in Sect. 2. Validation of coherent eddies, including roll vortices and other large turbulent eddies, is discussed in Sect. 3. A structural analysis and genesis mechanism are provided in Sect. 4. Diagnoses of the maintenance mechanism of large turbulent eddies are provided in Sect. 5. Conclusions are presented in Sect. 6.

2 Simulation Description

2.1 The WRF-LES Model

As described in Li et al. (2021), the one-way nested WRF model (version 3.9.1.1) with LES was used to simulate Hurricane Harvey (2017) during its landfall from 06 UTC 25 to 18 UTC 27 August 2017. In the model, the US National Centers for Environmental Prediction (NCEP) Global Forecast System (GFS) final analysis (FNL) $0.25^\circ \times 0.25^\circ$ data were used to derive the initial and boundary conditions. The YSU PBL scheme (Hong et al. 2006) was used in the first two domains, while the inner two domains used LES directly with the TKE 1.5 closure sub-scale turbulence scheme. These four domains were configured with grid meshes (horizontal resolution) of 150×150 (12.5 km), 251×281 (2.5 km), 951×1131 (0.5 km), and 1401×1401 (0.1 km), respectively. For the 71 vertical levels, over 39 levels were below 1500 m, with a minimum height of approximately 3 m. Domain 4 was moved with time to follow the hurricane. Configuration details can be found in Li et al. (2021).

2.2 Derivation of the Turbulence Field

As described in Li et al. (2021), the turbulence in LES is derived from the simulation result by subtracting the smoothed fields produced from the horizontal two-dimensional Gaussian filter:

$$G(x, y) = \frac{1}{2\pi\sigma^2} e^{-\frac{x^2+y^2}{2\pi\sigma^2}}, \quad (1)$$

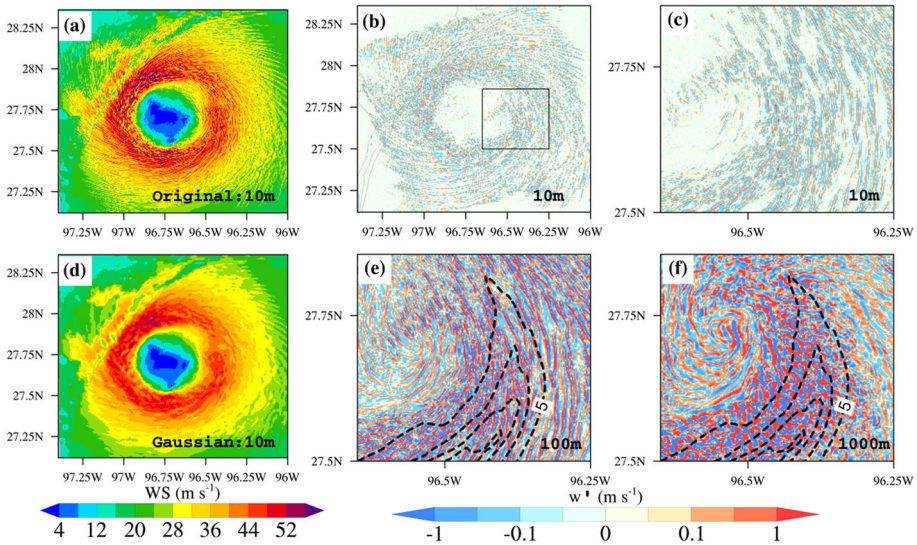


Fig. 1 10 m wind speed from the simulation conducted with **a** LES, **d** LES after smoothing by the Gaussian filter, **b** the turbulence w field by subtracting the smooth field generated by the Gaussian filter from LES, and enlarged map of the turbulence w field at a height of **c** 10 m, **e** 100 m, and **f** 1000 m at 01 UTC 26 August 2017. The black box in **b** represents the location of **c**, **e**, and **f**. The dashed contour line in **e–f** represents the rainband with contour interval of 10 mm h^{-1}

where x and y are the grids in the x and y directions. The bandwidth indicates the filter region was set at a 25×25 grid for domain 4 with a Gaussian function standard deviation σ of 10. Variables such as wind speed component u , v , w , and pressure were smoothed through the equation.

Figure 1a and d shows the 10 m wind speed from the original simulation conducted with LES and the simulation results after smoothing by the Gaussian filter, respectively, at 01 UTC 26 August 2017. The smoothed field (Fig. 1d) retains the hurricane structure and smooths out the perturbations. Therefore, the turbulence field can be computed by subtracting the smoothed field (e.g., Fig. 1d) from the original simulated field (e.g., Fig. 1a). In addition, the sensitivity of filtering results to the filter region was examined by varying the filter region to 50×50 grid. The results (not shown) are similar to those in Fig. 1, confirming the usefulness of the filtering method described in Eq. (1). Hereafter, we use these turbulence fields produced by subtracting the smoothed field generated by Eq. (1) from the original simulations to analyze the turbulence structure in LES.

3 Coherent Eddies: Roll Vortices Versus Large Turbulent Eddies

3.1 Structure of Turbulence Fields

LI et al. (2021) found that turbulence was reasonably resolved with roll vortices in domain 4 of the WRF-LES simulation. The turbulence in LES leads to strong wind perturbations, resulting in a higher surface wind that is consistent with the observations in Wurman and

Kosiba (2018) and Fernández-Cabán et al. (2019) for Hurricane Harvey. In this study, we focus on domain 4 to analyze the roll vortices and other eddies.

Figures 1b, c and 2a–d show the 10 m turbulence of w (Fig. 1b, c), u_r (inflow, Fig. 2a, c), and u_t (tangential wind, Fig. 2b, d) at 01 UTC 26 August 2017. Compared to Fig. 1d, many perturbations throughout the entire storm nearly align with the mean wind. A partially enlarged view in Figs. 1c and 2c, d shows that these perturbations are associated with updraft and downdraft turbulence that aligns along the mean wind direction and rotationally downstream of the storm center. The coupled positive and negative inflow and tangential turbulence along the mean wind direction combined with the coupled updraft and downdraft turbulence organize a spiraling turbulent eddy extending along the mean wind direction to the storm center.

To reveal the turbulence vertical structure, Fig. 1c, e, and f show the w' fields at different heights from 10 to 1000 m at 01 UTC 26 August 2017. With increasing height from 10 to 100 m, w' is gradually enhanced in the hurricane boundary layer and the turbulent eddy always nearly aligns with the mean wind direction. When the radius is reduced to the storm center, spiraling turbulent eddies throughout the storm boundary layer gradually converge along the storm flow field, and the strong convergence makes the well-structured spiraling turbulent eddy relatively chaotic near the eyewall. At a height of 1000 m, the well-structured spiraling turbulent eddy nearly disappears, but there is a strong chaotic turbulent eddy near the eyewall. There is no clear relationship between the rainband (dashed contour line) and the turbulent eddy. The distribution of rainband did not affect the distribution of strong turbulence in the hurricane. Hurricane observations from Guimond et al. (2018) reveal that strong turbulence exists near the eyewall and can extend upward to over 1000 m. The simulation here produces

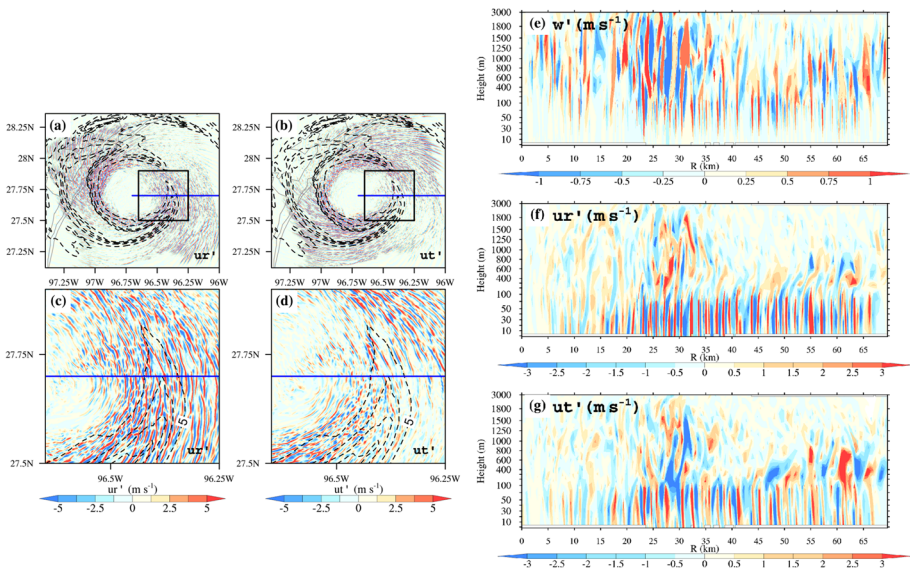


Fig. 2 10 m turbulence of inflow (a and c), tangential wind (b and d), and a cross section, along the blue line in (a–d) of the turbulent eddy vertical (e), radial (f), and tangential component (g) at 01 UTC 26 August 2017. X-axis in (e–g) represent the radius to the hurricane center. The black box in a, b represents the location of c, d. The dashed contour line in a–d represents the rainband with a contour interval of 10 mm h^{-1}

this turbulence structure well and demonstrates an accurate turbulence field with the Gaussian filter.

Figure 2e–g illustrates a cross section, along the blue line in Fig. 2a, of the turbulent eddy vertical (Fig. 2e), radial (Fig. 2f), and tangential component (Fig. 2g) at 01 UTC 26 August 2017. Consistent with the turbulence map, w' , u_r' , and u_t' all have coupled positive and negative values along the cross-section line below a height of 200 m, similar to observations in Morrison et al. (2005), indicating quasi-steady-state turbulent eddies, namely, roll vortices (rolls hereafter). These rolls can extend from near the surface to 200–400 m. Further, near the eyewall (radius of 20–40 km), there are strong perturbations above the rolls extending from approximately 200 m to over 1000 m, even to around 3000 m. These large turbulent eddies (eddies hereafter) are associated with rolls but are different from previous roll observations (Morrison et al. 2005) and simulations (Gao and Ginis 2014, 2016), which focused on rolls relatively far away from the storm center. However, these eddies are very similar to the turbulent eddies observed near the hurricane eyewall (Guimond et al. 2018). We found that these strong eddies can connect to the regular rolls near the top of the roll. This connection can also be found away from the storm center but usually has weaker eddy than that near the eyewall. LeMone (1973) suggested that mesoscale turbulence or structure can interact with rolls. Therefore, in the LES simulation presented in this study, eddies (200–1000 m) are associated with rolls (from near the surface to 200 m) and form coherent eddies (including rolls and eddies) near the eyewall from near the surface to 1000 m and even beyond (~3000 m).

3.2 Wavelength

The wavelength varies in different turbulent structures (Young et al. 2002; Foster 2005). To distinguish the differences and examine the connection between eddies and rolls, the wavelengths of strong eddies and rolls are compared. As shown in Fig. 1f and 2e–g, strong eddies occur mainly within a 20–40 km radius of the storm center and extend upward from approximately 200 m to over 1000 m. We examined four cross-section lines from the hurricane center to the north, east, south, and west at heights of 100 m and 1000 m during the simulation period to obtain roll and eddy perturbations, respectively. The w' is considered an eddy at a height of 1000 m and an roll at a height of 100 m over an area within a radius of 20–40 km.

Since rolls and eddies both have coupled upward and downward turbulence motion, the wavelength is detected by the distance between two adjacent local maxima or minima of the cross-section data. Figure 3a shows an example of the probability distribution of the wavelength of rolls within a radius of 20–40 km and 40–100 km at a height of 100 m during hurricane landfall at 00–02 UTC on 26 August. The wavelengths based on local maxima and minima are both shown in the figure. The probability distributions of wavelengths at different radii from the local maxima and minima are close to each other, with wavelength maxima at around 0.5–1.5 km and a mean wavelength of 0.8 km. This wavelength is slightly different from the mean wavelength of about 1.6 km found by Morrison et al. (2005) but is the same as that in Huang et al. (2018), who observed an approximately 1 km wavelength roll in the same region through radar and satellite observations. The similar wavelength probability distributions of rolls at different radii, i.e., 20–40 km and 40–100 km, indicate that the structure of rolls is the same near the eyewall and away from the eyewall. Furthermore, the distribution of wavelength of rolls did not change (change less than 1%) for different filter region choices (not shown), indicating that the scale of the rolls is conserved with respect to filter region. With a depth of approximately 200–400 m (Fig. 2e–g) and a mean wavelength of

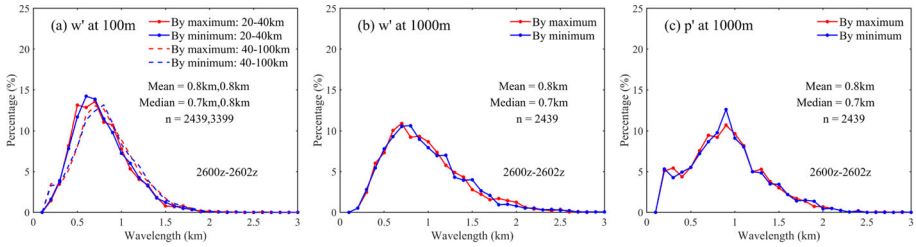


Fig. 3 Probability distribution of the wavelength of **a** rolls within a radius of 20–40 km and 40–100 km at a height of 100 m, **b** eddies within a radius of 20–40 km at a height of 1000 m, and **c** pressure perturbation within a radius of 20–40 km at a height of 1000 m during hurricane landfall at 00–02 UTC on 26 August. The red and blue lines represent the probability distributions detected by local maxima and minima, respectively. The global mean, median, and number (n) are also shown

0.8 km, the roll aspect of 2–4 confirms that the LES-simulated rolls are close to the summary by Young et al. (2002), who found that roll aspect varied from 2 to 6 with a PBL height of around 200 m.

For eddies, Fig. 3b shows an example of the probability distribution of wavelengths within a radius of 20–40 km at a height of 1000 m during hurricane landfall at 00–02 UTC 26 August. The probability distributions of wavelengths from local maxima and minima are close to each other, with global maxima around 0.5–1.5 km and a mean wavelength of 0.9–1.1 km, which is very close to the observations of Guimond et al. (2018). Compared to the rolls, the wavelength probability distributions of eddies have a slightly lower percentage in the 0.5–1 km wavelength range (10% to eddies and 15% to rolls). Apart from this difference, the similar probability distributions of wavelengths between eddies and rolls indicate the connection between eddies and rolls near the eyewall.

To understand the generation and evolution of these coherent eddies, including both rolls and eddies, in the following sections, we examine their structure and mechanism.

4 Evolution and Genesis of Coherent Eddies

4.1 Evolution of Roll Vortices and Turbulence

To examine the evolution of rolls and eddies, Fig. 4 shows the azimuthally averaged vertical turbulence intensity (namely, $I_w = w'^2/2$, contour line, w' is the turbulence vertical component) before Hurricane Harvey's landfall at 12 UTC (Fig. 4a), 17 UTC (Fig. 4b), and 22 UTC (Fig. 4c) on 25 August 2017; during its landfall at 01 UTC (Fig. 4d), 05 UTC (Fig. 4e), and 09 UTC (Fig. 4f) on 26 August 2017; and after its landfall at 14 UTC (Fig. 4g) and 19 UTC (Fig. 4h) on 26 August, and from 00 UTC (Fig. 4i) on 27 August 2017. The maximum 10-m wind speed (MWS) at each time is also shown. Before hurricane landfall, the strong I_w , including rolls and eddies, extends from a height of about 75 m to 3000 m. With hurricane intensification, MWS increases from 51 to 73 $\text{m}\cdot\text{s}^{-1}$, and I_w also increases, with a maximum of over 1–4 $\text{m}^2\cdot\text{s}^{-2}$. During hurricane landfall, the hurricane gradually decays and MWS decreases from 72 to 54 $\text{m}\cdot\text{s}^{-1}$. The turbulence height (with I_w greater than 0.5 $\text{m}^2\cdot\text{s}^{-2}$) for eddies gradually reduces from a height of over 3000 m to about 2500 m. Maximum I_w reduces from over 4 $\text{m}^2\cdot\text{s}^{-2}$ to 2 $\text{m}^2\cdot\text{s}^{-2}$. Inland, as the hurricane decays, MWS gradually decreases from 34 to 26 $\text{m}\cdot\text{s}^{-1}$, and the strong coherent eddies (rolls and eddies) almost

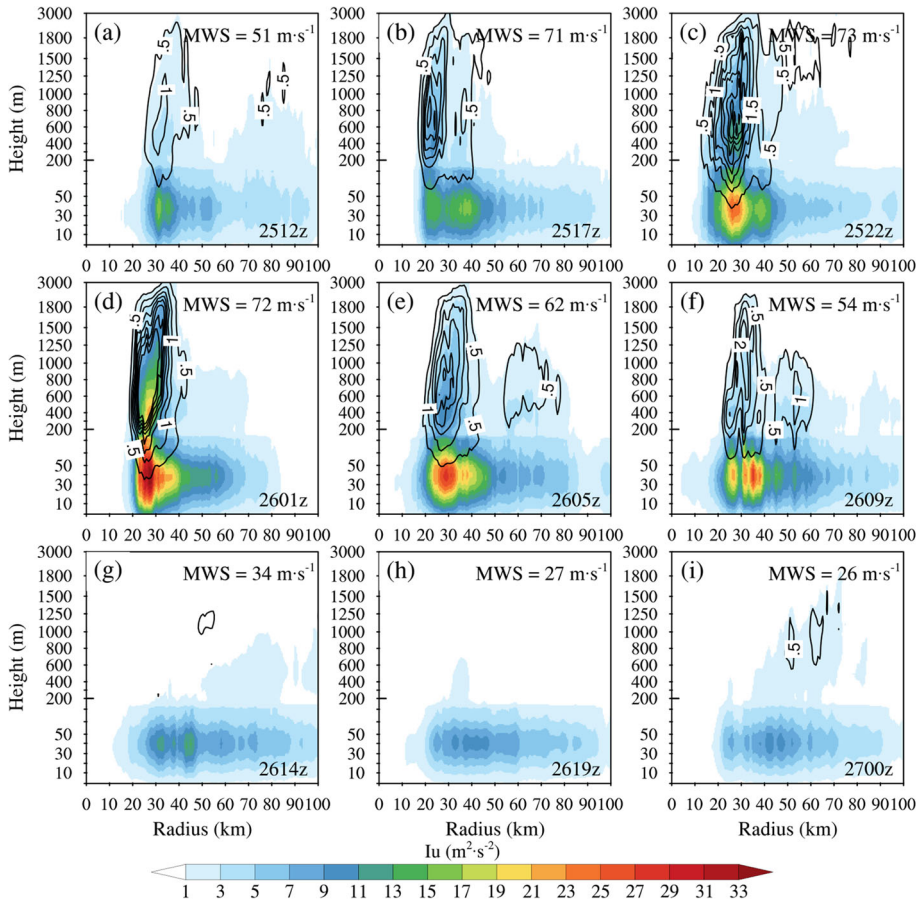


Fig. 4 Azimuthally averaged horizontal turbulence intensity (I_u , shaded) and vertical turbulence intensity (I_w contour line with interval of $0.5 \text{ m}^2 \text{ s}^{-2}$) before hurricane landfall at 12 UTC (a), 17 UTC (b), and 22 UTC (c) on 25 August; during landfall at 01 UTC (d), 05 UTC (e), and 09 UTC (f) on 26 August; and after landfall at 14 UTC (g) and 19 UTC (h) on 26 August, and from 00 UTC (i) on 27 August. The 10-m maximum wind is also shown

disappear, with maximum I_w of less than $1 \text{ m}^2 \text{ s}^{-2}$. Although the rolls seem to disappear after landfall, some rolls still exist (Morrison et al. 2005; Li et al. 2021), but they are too weak to show in the figures.

During the simulation period, although rolls prevail over the entire hurricane boundary layer (Figs. 1 and 2), rolls are weak away from the eyewall, which makes azimuthally averaged I_w usually less than $0.5 \text{ m}^2 \text{ s}^{-2}$. The I_w near the eyewall is proportional to hurricane intensity (MWS), while the I_w distribution along the radius is not proportional to wind speed. Along the radius, wind speed can be reduced to only half the maximum at a radius of 70–80 km, while I_w can be reduced to less than one-eighth of the maximum I_w .

Horizontal turbulence is also analyzed in Fig. 4, which shows the azimuthally averaged horizontal turbulence intensity (namely, $I_u = (u_r'^2 + u_t'^2)/2$, shaded; u_r' is the turbulence radial component; u_t' is the turbulence tangential component) before (Fig. 4a–c), during (Fig. 4d–f), and after hurricane landfall (Fig. 4g–i). Before landfall, under strong I_w , there

is always a strong I_u associated with rolls at heights below 200 m, with a maximum of over $15 \text{ m}^2 \text{ s}^{-2}$ below 200 m. Within the region of strong I_w , eddy-associated I_u is relatively weak, with a maximum of over $3 \text{ m}^2 \text{ s}^{-2}$. During landfall, I_u below 200 m gradually reduces from a maximum of over $33\text{--}27 \text{ m}^2 \text{ s}^{-2}$ with reduced MWS. Above 200 m, eddy-associated I_u also gradually decreases, with a maximum of over $21\text{--}5 \text{ m}^2 \text{ s}^{-2}$. After landfall, below 200 m, there is still horizontal turbulence, but it is also weakened, with maximum I_u decreasing from 13 to $9 \text{ m}^2 \text{ s}^{-2}$. Above 200 m, horizontal turbulence is the same as vertical turbulence and almost disappears, with maximum I_u less than $3 \text{ m}^2 \text{ s}^{-2}$.

Similar to vertical turbulence, horizontal turbulence near the eyewall, including turbulence contributed by eddies and rolls, is also proportional to hurricane intensity, while the decrease in I_u along the radius is significantly quicker than the decrease in wind speed. Although rolls usually extract energy from the mean flow (LeMone 1973; Foster 2005), the reduction of I_u and I_w along the radius is always quicker than that of wind speed in the simulation result. Therefore, the extremely intense coherent eddies (rolls and eddies) near the hurricane eyewall are not caused only by the strong wind there. The specific stream structure of the hurricane—namely, accumulation by horizontal convergence—may also be critical for extremely intense turbulent kinetic energy (TKE) near the eyewall. Meanwhile, roll-related I_u (below 200 m) is usually larger than that related to eddies, while roll-related I_w (below 200 m) is usually weaker than that related to eddies, indicating a different turbulent kinetic energy distribution of eddies and rolls.

4.2 Stability Conditions

Previous studies have found that rolls are often generated with a flux Richardson number (R_f) less than 0.25 (Gao and Ginis 2014). Near-neutral conditions can suppress a roll enhanced by convection (Foster 2005). To clarify the stability of thermodynamic conditions associated with rolls and eddies, azimuthally averaged R_f ($= \frac{g}{\theta_v} \langle w' \theta_v' \rangle / (\langle u' w' \rangle \frac{\partial \langle u \rangle}{\partial z} + \langle v' w' \rangle \frac{\partial \langle v \rangle}{\partial z})$) at the same time as in Fig. 4 is shown in Fig. 5 before (Fig. 5a–c), during (Fig. 5d–f), and after hurricane landfall (Fig. 5g–i). *The height of the thermodynamic hurricane boundary layer is determined by the height where the potential temperature gradient is over 3 K km^{-1} with a temperature inversion above to create a potential temperature difference of over 2 K (Heffter 1980).* This calculated hurricane boundary layer height (HBLH) is also azimuthally averaged and added in Fig. 5. For convenience, azimuthally averaged I_w , representing coherent eddy rolls and eddies, and I_u (dashed line), which majorly representing rolls, are also displayed in Fig. 5 as contour lines.

From Fig. 5, we found that before landfall, rolls and eddies are generated mainly with R_f at -0.2 to 0.2 . Only a small region has rolls and eddies with R_f exceeding this threshold. The HBLH always has a lower value of about 200 m in the region where strong rolls and eddies prevail. The main part of eddies is always above the HBLH. During landfall, rolls and eddies gradually decay where R_f gradually exceeds the threshold of -0.2 to 0.2 . The HBLH also has a lower value in the roll-prevailing region except at 09 UTC 26 August, when a lower HBLH is located near the storm center. After landfall, although the strong rolls and eddies almost disappear, some regions still have R_f within the threshold of -0.2 to 0.2 . The HBLH is almost unchanged at about 200 m, except in the eye center. During the simulation period, there are suitable thermodynamic conditions for rolls with R_f within -0.2 to 0.2 . After landfall, these suitable conditions still exist, but strong rolls and eddies disappear. Results here indicate that thermodynamic conditions are necessary but not sufficient for the generation of strong rolls and eddies near the hurricane eyewall.

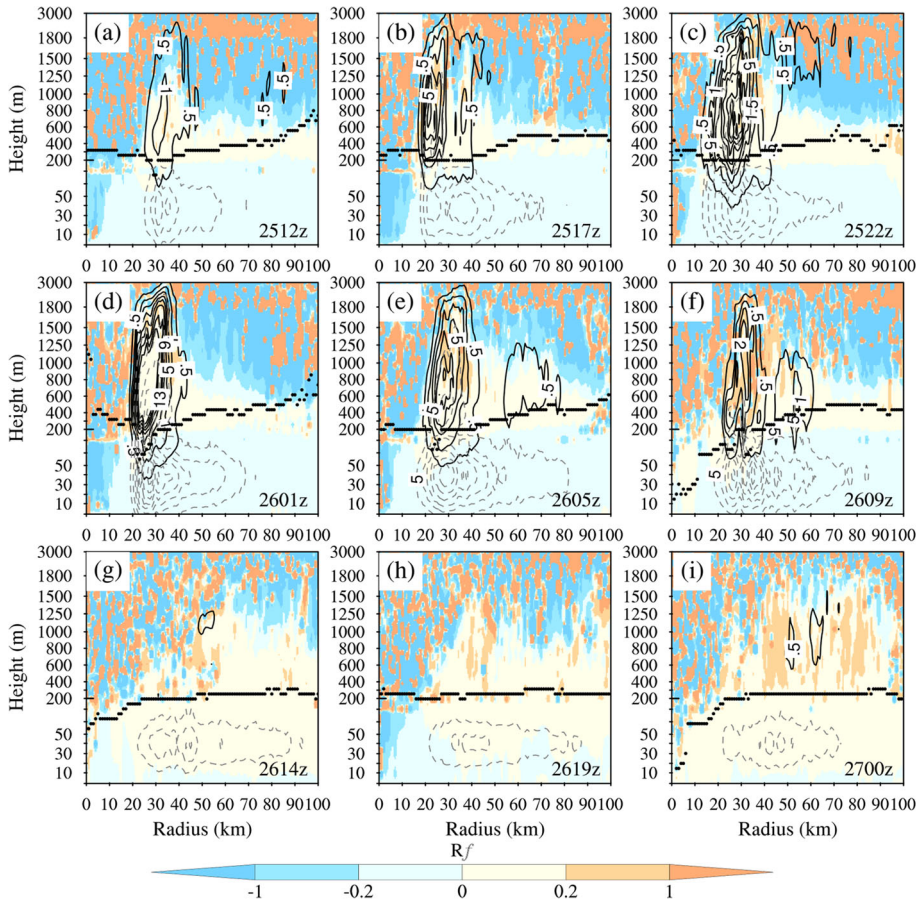


Fig. 5 Similar to Fig. 4 but for the azimuthally averaged flux Richardson number (R_f). The azimuthally averaged thermodynamic hurricane boundary layer height is also shown, and the related azimuthally averaged I_w (solid line, with a contour interval of $0.5 \text{ m}^2 \text{ s}^{-2}$) and I_u (dashed line, with a contour interval of $4 \text{ m}^2 \text{ s}^{-2}$) are added as a contour line

Foster (2005) pointed out that a dynamic condition—namely, radial wind inflection point instability in the hurricane boundary layer—is fundamental for the generation of rolls. To investigate this dynamic condition, the azimuthally averaged radial wind shear (positive for inflow) at the same time as in Fig. 4 is shown in Fig. 6 before (Fig. 6a–c), during (Fig. 6d–f), and after hurricane landfall (Fig. 6g–i). Azimuthally averaged I_w and I_u are also added to the figure to distinguish the eddies and rolls near the eyewall. We see that during the whole simulation period, strong negative inflow wind shear covers the main part of rolls (height of 30–200 m). The negative inflow wind shear is distributed all around the storm boundary layer and is consistent with the prevailing rolls shown in Figs. 1 and 2. The strong negative inflow wind shear is related to the strong dynamic instability. This inflow wind shear gradually enhances from an intensity of -0.08 to over -0.12 s^{-1} with hurricane intensification. During hurricane landfall, within a radius of 0–20 km in the hurricane eye region, there is also a strong negative inflow wind shear, with a minimum of less than -0.12 s^{-1} . This strong

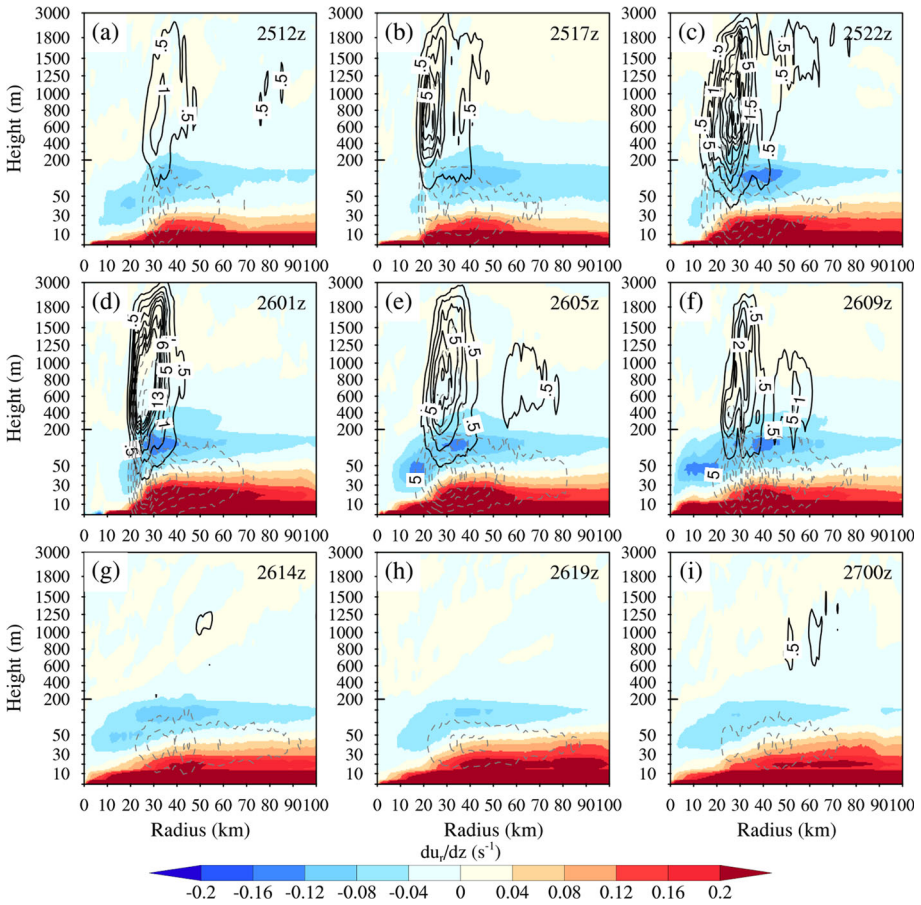


Fig. 6 Similar to Fig. 4 but for the azimuthally averaged inflow wind shear. The azimuthally averaged I_w (solid line, with a contour interval of $0.5 \text{ m}^2 \text{ s}^{-2}$) and I_u (dashed line, with a contour interval of $4 \text{ m}^2 \text{ s}^{-2}$) are added as a contour line

negative inflow wind shear results in the growth of strong roll instability, while no strong rolls exist there. Considering the unfavorable thermodynamic conditions shown in Fig. 5 in this strong negative inflow wind shear region, very stable or unstable stratification suppresses the generation of rolls there (Foster 2005). After landfall, the strong rolls almost disappear even though there is still negative inflow wind shear with a minimum of less than -0.08 s^{-1} .

The inflow wind shear is the genesis of the hurricane roll (Foster 2005; Gao and Ginis 2014). However, the dynamic instability and thermodynamic conditions here cannot explain the large I_w associated with extremely intense rolls and eddies that exist near the hurricane eyewall but explain only the prevailing rolls in the entire hurricane boundary layer (Figs. 1 and 2). Other mechanisms of the hurricane, e.g., accumulation by horizontal convergence, may be critical for extremely intense TKE near the eyewall.

4.3 Convergence of Inflow

With strong inflow in the hurricane boundary layer, mass convergence and accumulation near the eyewall are observed. The impact of inflow convergence near the eyewall is analyzed in Fig. 7, which shows the horizontal divergence of the azimuthally averaged inflow (du_r/dr ; u_r represents the inflow while the positive values for inflow) at the same time as in Fig. 4 before (Fig. 7a–c), during (Fig. 7d–f), and after hurricane landfall (Fig. 7g–i). The r-axis points to the center of the hurricane. Similarly, the azimuthally averaged I_w and I_u are also added to Fig. 7 as strong eddies and rolls with contour lines. From the figures, we see that there is always a strong negative du_r/dr covering the main part of the strong rolls below 200 m with a minimum of less than $-2 \times 10^{-3} \text{ s}^{-1}$. This strong negative du_r/dr indicates strong inflow convergence near the eyewall. During landfall, the strong inflow convergence region with a minimum of less than $-2 \times 10^{-3} \text{ s}^{-1}$ still covers the main part of the strong rolls near the eyewall. After landfall, the convergence is weak, with a minimum of more than $-$

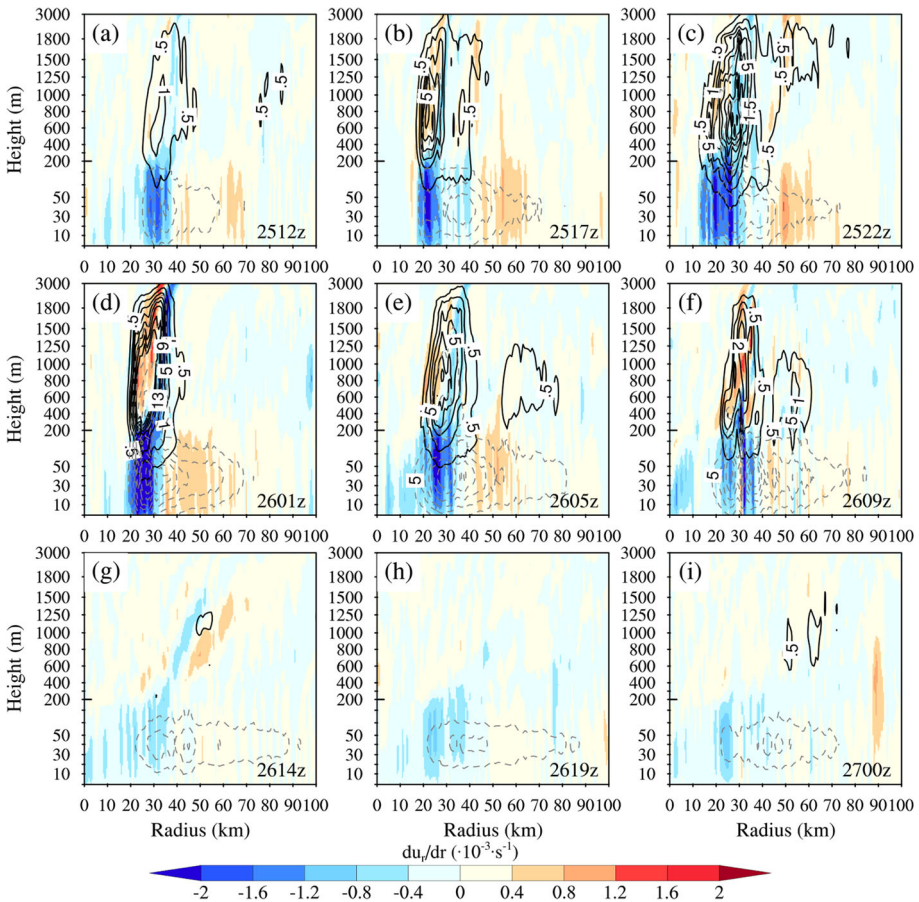


Fig. 7 Similar to Fig. 4 but for the horizontal divergence of azimuthally averaged inflow (du_r/dr). The azimuthally averaged I_w (solid line, contour interval $0.5 \text{ m}^2 \text{ s}^{-2}$) and I_u (dashed line, contour interval $4 \text{ m}^2 \text{ s}^{-2}$) are added as a contour line

$1.2 \times 10^{-3} \cdot s^{-1}$, related to the near disappearance of the strong eddies and rolls. Therefore, inflow convergence near the eyewall is critical for the strong eddies and rolls in the hurricane. Horizontal convergence is significantly related to the horizontal advection effect, and there is clearly roll horizontal advection through the horizontal wind from some distance away to near the eyewall, as shown in Figs. 1 and 2a–d. The inflow transports the rolls in the entire storm boundary layer and accumulates near the eyewall to support the intense rolls there. Once the horizontal transport, especially the inflow, gradually decays after hurricane landfall, the TKE accumulation mechanism is also gradually destroyed.

Based on this relationship of horizontal convergence and coherent eddies, Li and Pu (2021) parameterized hurricane turbulence near the eyewall with the WRF model through convergence and added the vertical mixing contributions of rolls and eddies in a modified PBL scheme. The better hurricane forecast from the WRF model with the modified PBL scheme confirmed that horizontal convergence near the eyewall is critical for forming the intense rolls and eddies in a hurricane (see details in Li and Pu 2021).

5 Maintenance of the Vertical Motion of Rolls and Eddies

Although we have known that inflow convergence transports roll turbulence to near a storm’s eyewall, it is unclear how this horizontal advection supports the vertical motion of turbulence near the eyewall, especially for the strong vertical component of eddies, which can strongly change vertical mixing near the eyewall (Zhang and Drennan 2012; Zhao et al. 2020; Li et al. 2021). To this end, Table 1 shows a summary of the magnitude of the wind shear term, buoyancy term, and pressure transport term, all of which can contribute to the TKE, during the simulation based on the following equations:

$$\begin{aligned} \frac{\partial \langle u'^2 \rangle}{\partial t} = & -2\langle u'w' \rangle \frac{\partial \langle u \rangle}{\partial z} - 2\langle u'v' \rangle \frac{\partial \langle u \rangle}{\partial y} - \langle w \rangle \frac{\partial \langle u'^2 \rangle}{\partial z} - \langle v \rangle \frac{\partial \langle u'^2 \rangle}{\partial y} \\ & - \frac{\partial \langle u'^2 w' \rangle}{\partial z} - \frac{\partial \langle u'^2 v' \rangle}{\partial y} - \frac{2}{\langle \rho \rangle} \frac{\partial \langle u'P' \rangle}{\partial x} - 2\varepsilon, \end{aligned} \tag{2}$$

Table 1 Summary of the magnitude of the TKE contribution by the wind shear term, buoyancy term, and pressure transport term

Magnitude	Horizontal wind shear term	Vertical wind shear term	Buoyancy term	Pressure transport term
	$-\langle u'w' \rangle$ $du/dz - \langle u'v' \rangle$ du/dy	$-\langle u'w' \rangle$ dw/dx	$g \langle w'\theta'_L \rangle / \theta_L$	$d \langle w'P' \rangle / \rho dz$
	$-\langle v'w' \rangle$ $dv/dz - \langle u'v' \rangle$ dv/dx	$-\langle v'w' \rangle dw/dy$		
Rolls	$0.4 \text{ m}^2 \text{ s}^{-3}$	$\pm 0.001 \text{ m}^2 \text{ s}^{-3}$	$- 0.001 \text{ m}^2 \text{ s}^{-3}$	$\pm 0.4 \text{ m}^2 \text{ s}^{-3}$
Eddies	$0.2 \text{ m}^2 \text{ s}^{-3}$	$\pm 0.001 \text{ m}^2 \text{ s}^{-3}$	$- 0.008 \text{ m}^2 \text{ s}^{-3}$	$\pm 0.4 \text{ m}^2 \text{ s}^{-3}$

$$\begin{aligned} \frac{\partial \langle v'^2 \rangle}{\partial t} = & -2 \langle v' w' \rangle \frac{\partial \langle v \rangle}{\partial z} - 2 \langle u' v' \rangle \frac{\partial \langle v \rangle}{\partial x} - \langle w \rangle \frac{\partial \langle v'^2 \rangle}{\partial z} - \langle u \rangle \frac{\partial \langle v'^2 \rangle}{\partial x} \\ & - \frac{\partial \langle v'^2 w' \rangle}{\partial z} - \frac{\partial \langle v'^2 u' \rangle}{\partial x} - \frac{2}{\langle \rho \rangle} \frac{\partial \langle v' P' \rangle}{\partial y} - 2\varepsilon, \end{aligned} \quad (3)$$

$$\begin{aligned} \frac{\partial \langle w'^2 \rangle}{\partial t} = & -2 \langle u' w' \rangle \frac{\partial \langle w \rangle}{\partial x} - 2 \langle v' w' \rangle \frac{\partial \langle w \rangle}{\partial y} - \langle u \rangle \frac{\partial \langle w'^2 \rangle}{\partial x} - \langle v \rangle \frac{\partial \langle w'^2 \rangle}{\partial y} \\ & - \frac{\partial \langle w'^2 u' \rangle}{\partial x} - \frac{\partial \langle w'^2 v' \rangle}{\partial y} + \frac{g}{\theta_L} \langle w' \theta'_L \rangle - \frac{2}{\langle \rho \rangle} \frac{\partial \langle w' P' \rangle}{\partial z} - 2\varepsilon. \end{aligned} \quad (4)$$

On the right-hand side, terms 1 and 2 represent horizontal wind shear (in Eqs. 2 and 3) and vertical wind shear (in Eq. 4), term 3 and 4 in Eqs. 2–4 represent transport contributions that are very weak and neglected in this study. The last term represents the dissipation in Eqs. 2–4. In Eqs. 2–4, only a few terms contribute to the vertical motion of turbulence. The contribution details by the wind shear term, the buoyancy term, and the pressure transport term that are discussed in this section to verify the energy support for the vertical motion of rolls and eddies. Note that the equation should consider the contribution of both mesoscale and mean winds. In this study, the result from the Gaussian filter shows a very small change (less than 1%) to the detrend result, indicating the remove of the mesoscale impact. Therefore, the mesoscale contribution is neglected in Eq. 2–4 and in the following discussion.

5.1 Energy Support

Figure 8 shows the azimuthally averaged horizontal wind shear term at the same time as in Fig. 4 before (Fig. 8a–c), during (Fig. 8d–f), and after hurricane landfall (Fig. 8g–i). Before landfall, in the region of strong rolls, the wind shear term is positive and gradually enhances, from a maximum of over $0.2\text{--}0.4 \text{ m}^2 \text{ s}^{-3}$. This positive wind shear term supports the strong rolls in the hurricane boundary layer (Foster 2005; Gao and Ginis 2014). In the region of strong eddies, the wind shear term can only reach a maximum of over $0.2 \text{ m}^2 \text{ s}^{-3}$. The maximum of $0.4 \text{ m}^2 \text{ s}^{-3}$ ($0.2 \text{ m}^2 \text{ s}^{-3}$) is considered to be the magnitude of the contribution of the horizontal wind shear term to rolls (eddies), as summarized in Table 1. During landfall, the wind shear term is still positive around the region of strong rolls and eddies and gradually weakens. After landfall, similar to the strong eddies, wind shear is weak, with the maximum gradually decreasing to less than $0.1 \text{ m}^2 \text{ s}^{-3}$.

Although the horizontal wind shear is strong, it does not directly generate vertical velocity associated with rolls and eddies (Fig. 4) (Zhou et al. 2019). The vertical wind shear term (not shown), which supports the vertical component of TKE associated with rolls and eddies (Fig. 4), is extremely weak, usually negative, and less than $0.001 \text{ m}^2 \text{ s}^{-3}$ (magnitude of the vertical wind shear term contribution shown in Table 1). Therefore, the wind shear does not support the vertical component of TKE associated with strong rolls and eddies.

To clarify the energy support for the vertical component of TKE, Fig. 9 shows the azimuthally averaged buoyancy term $g < w' \theta'_L > / \theta_L$ at the same time as in Fig. 4 before (Fig. 9a–c), during (Fig. 9d–f), and after hurricane landfall (Fig. 9g–i). Effects of the water vapor, cloud water, and rain water are considered in the buoyancy term. Before landfall, around the region of strong eddies, the buoyancy term $g < w' \theta'_L > / \theta_L$ is negative and gradually enhances, from a minimum of less than $-0.003 \text{ m}^2 \text{ s}^{-3}$ to less than $-0.008 \text{ m}^2 \text{ s}^{-3}$ (the

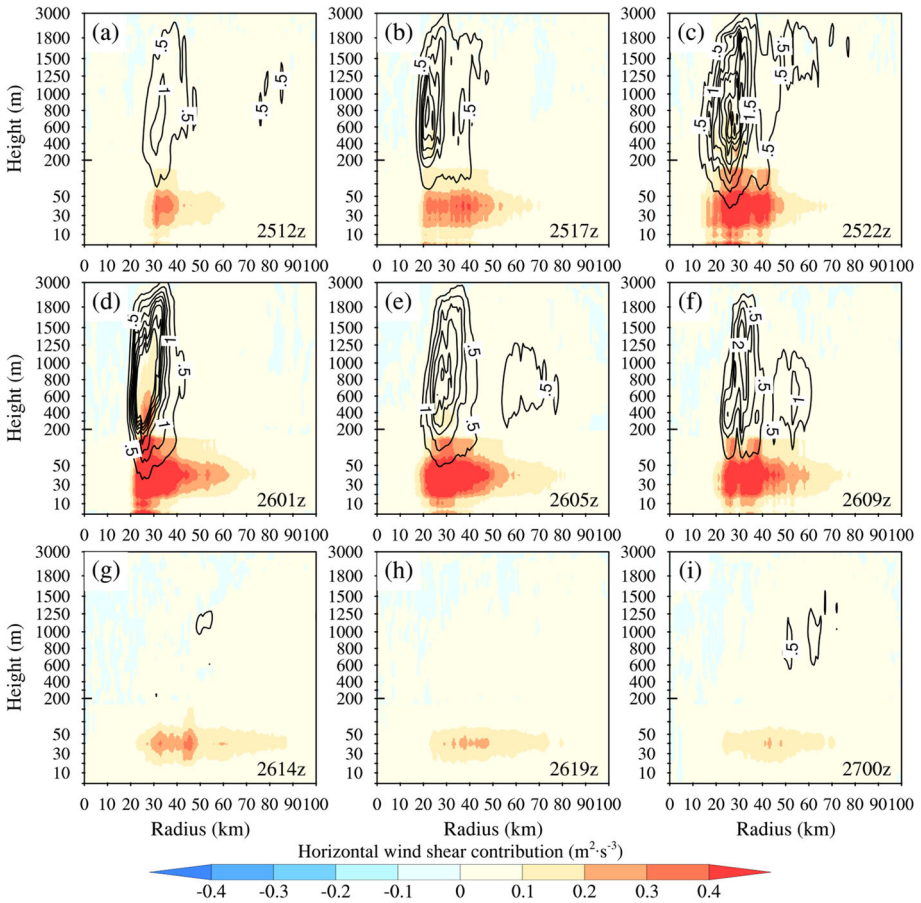


Fig. 8 Similar to Fig. 4 but for the horizontal wind shear contribution to TKE. The azimuthally averaged I_w is added as a contour line

magnitude of the buoyancy term contribution to eddies is shown in Table 1). This negative buoyancy term reflects a suppression effect on the vertical motion of strong eddies in the hurricane boundary layer. In the region of rolls, the buoyancy term $g < w'\theta'_L > / \theta_L$ is very weak, with a minimum of $-0.001 \text{ m}^2 \text{ s}^{-3}$ (the magnitude of the buoyancy term contribution to rolls is shown in Table 1). During landfall, $g < w'\theta'_L > / \theta_L$ is still negative around the region of strong eddies and gradually weakens. After landfall, similar to the strong eddies, $g < w'\theta'_L > / \theta_L$ is weak, with a minimum of less than $-0.003 \text{ m}^2 \text{ s}^{-3}$. Similar to rolls (Foster 2005; Lilly 1966; Brown 1980), the buoyancy term $g < w'\theta'_L > / \theta_L$ is not a significant factor for eddies, as its value is significantly less than that of the wind shear term. The term $g < w'\theta'_L > / \theta_L$ only slightly suppresses the generation of eddies.

5.2 Energy Transfer

Since the buoyancy term does not support the strong vertical motion of rolls and eddies, other transport terms in the TKE equation should be concerned with supporting the vertical

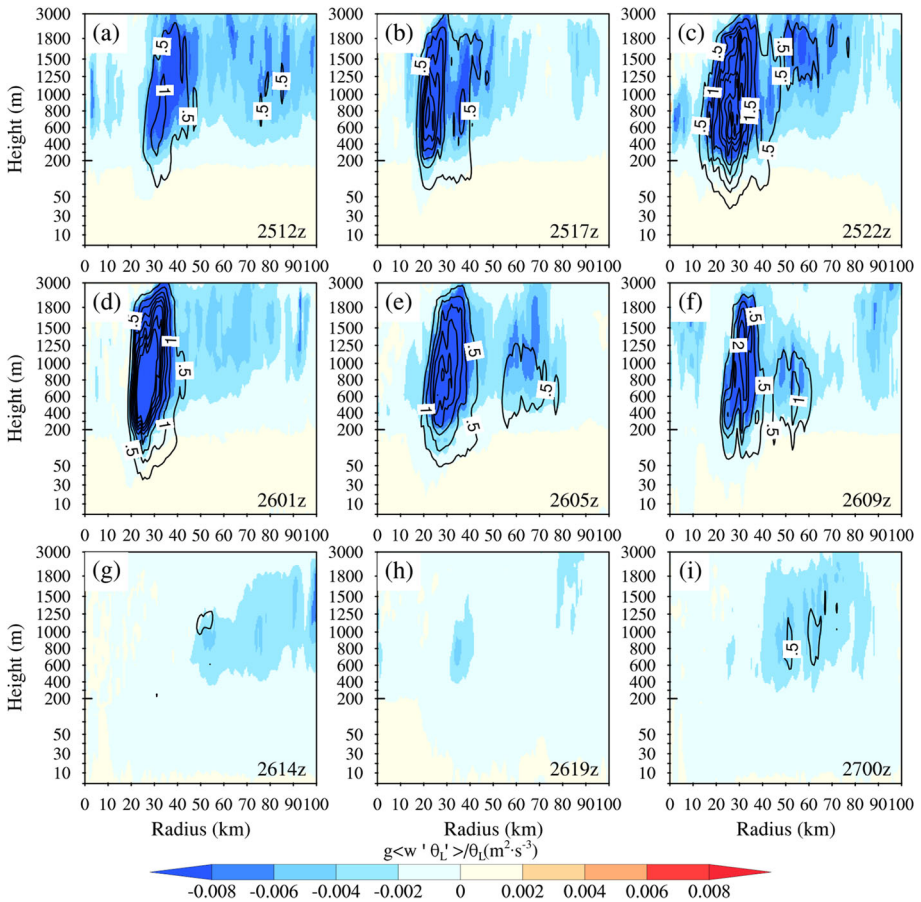


Fig. 9 Similar to Fig. 4 but for the azimuthally averaged buoyancy term $g < w'\theta'_L > / \theta_L$. The azimuthally averaged Iw is added as a contour line

component of TKE. Figure 10 shows the azimuthally averaged pressure transport term $d < w'P' > / \rho dz$ at the same time as in Fig. 4 before (Fig. 10a–c), during (Fig. 10d–f), and after hurricane landfall (Fig. 10g–i). Before landfall, there is a strong pressure transport term in the same region as large Iw . With hurricane intensification, the pressure transport term is enhanced, with a maximum of over $0.4 \text{ m}^2 \text{ s}^{-3}$ or a minimum of less than $-0.4 \text{ m}^2 \text{ s}^{-3}$, which enhances upward and downward turbulence, respectively. During landfall, the transport term is still strong, with a maximum of over $0.4 \text{ m}^2 \text{ s}^{-3}$ or a minimum of less than $-0.4 \text{ m}^2 \text{ s}^{-3}$ in the same region as large Iw , indicating a contribution of the pressure transport term of $\pm 0.4 \text{ m}^2 \text{ s}^{-3}$ (shown in Table 1). After landfall, the pressure transport term is weak but still exists, with a maximum of over $0.2 \text{ m}^2 \text{ s}^{-3}$ or a minimum of less than $-0.2 \text{ m}^2 \text{ s}^{-3}$. The strong eddies almost disappear.

Compared to the weak buoyancy term (one-tenth of a percent of the pressure transport or less), the pressure transport term dominates the vertical component of rolls and eddies. Since the pressure transport term can only transfer the horizontal component of turbulence to the vertical component, the quick decay of strong eddies after landfall cannot be attributed to

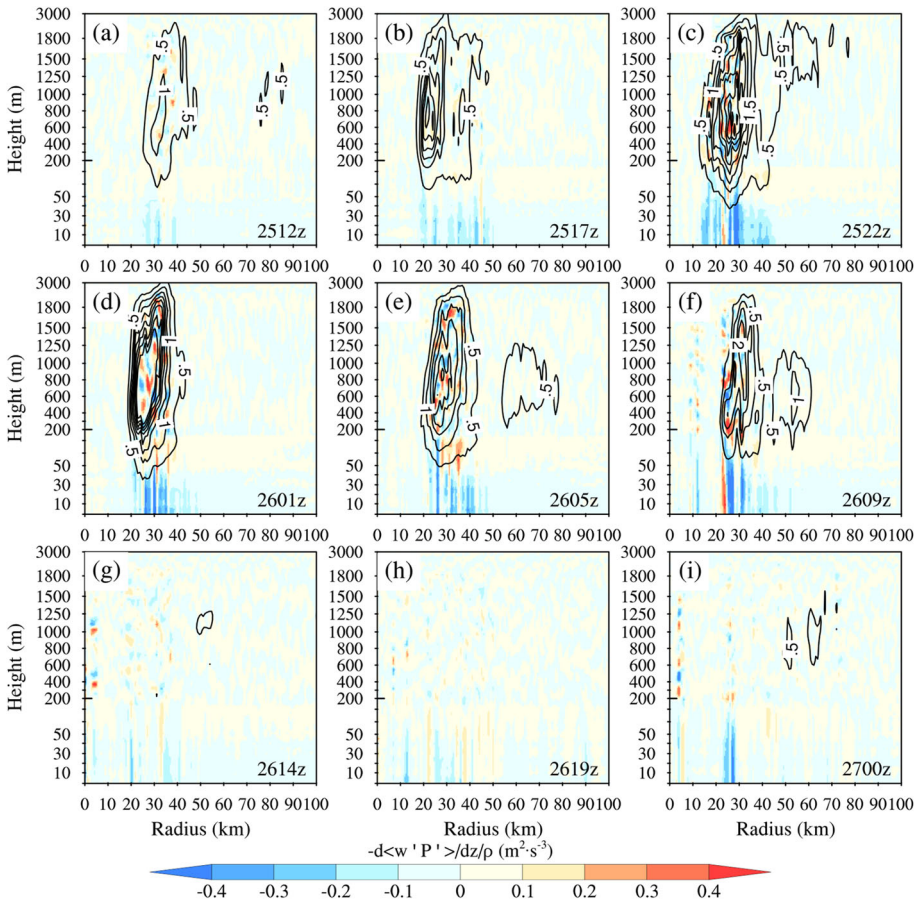


Fig. 10 Similar to Fig. 4 but for the azimuthally averaged pressure transport. The azimuthally averaged I_w is added as a contour line

the energy transport of the pressure transport term but to the decay of the horizontal wind shear term (Fig. 8g–i). Before and during landfall, the pressure transport term transfers the horizontal component of rolls and eddies to support the strong I_w at a height of 75–3000 m. The energy transfer through the pressure transport term, which covers the region of rolls and eddies, connects the vertical component of rolls and eddies, resulting in a similar wavelength structure shown in Figs. 3a, b.

From the definition, pressure transport in the TKE budget is associated with the vertical perturbation pressure gradient force and then controlled by pressure perturbation. The pressure is related mainly to air density and temperature through ideal gas law. To verify the contributions of these two factors, the indexes $\frac{P'\rho'}{\rho}$ and $\frac{P'T'}{T}$ represent the contributions of air density and air temperature perturbations to the pressure perturbation, are analyzed in Fig. 11. The larger index indicates a larger impact on pressure perturbation from air density and/or temperature. Figure 11 shows an example of the azimuthally averaged $\frac{P'\rho'}{\rho}$ and $\frac{P'T'}{T}$ during hurricane landfall at 0100 UTC on 26 August 2017. $\frac{P'\rho'}{\rho}$ is always positive, with

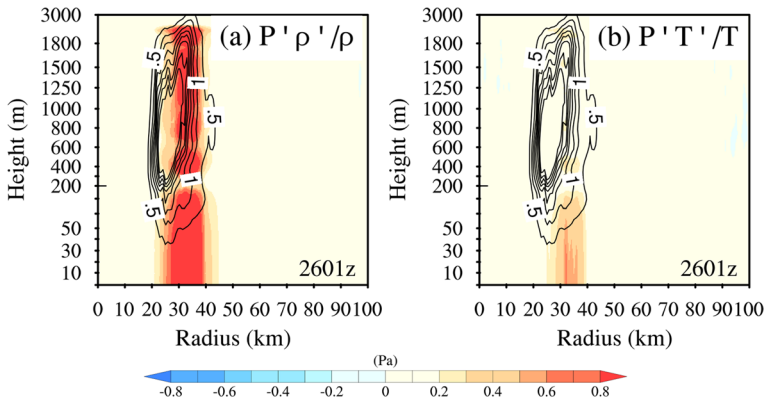


Fig. 11 Azimuthally averaged **a** $\frac{P'\rho'}{\rho}$ and **b** $\frac{P'T'}{T}$ during hurricane landfall at 01 UTC on 26 August 2017. The azimuthally averaged I_w is added as a contour line

a maximum of over 0.8 Pa, while the maximum $\frac{P'T'}{T}$ as well as the maximum coverage region are both smaller than that of $\frac{P'\rho'}{\rho}$. This reflects the positive and strong relationship between pressure perturbation and air density, and the weak impact of air temperature perturbation on pressure perturbation. As shown in Fig. 7, there is usually strong convergence near the eyewall. The density perturbation may be associated with this strong convergence there. Therefore, due to the strong horizontal convergence in the storm, there is some density perturbation that leads to pressure perturbation and finally mixes the vertical perturbation to enhance the I_w associated with rolls and eddies. The horizontal advection of rolls throughout the entire hurricane boundary layer is usually combined with the strong wind shear near the eyewall to create intense rolls there. Then, the pressure transport term transfers the TKE horizontal component to organize the vertical component of rolls and eddies near the hurricane eyewall. After hurricane landfall, the weak horizontal advection and weak wind shear reduce the energy support and decrease the strong coherent eddies, including rolls and eddies.

5.3 Wavelength

In this section, the wavelength of strong eddies and that of pressure perturbation are compared to clarify the connection between eddies and pressure perturbation. Four cross sections from the hurricane center to the north, east, south, and west at a height of 1000 m are examined at each time to obtain pressure perturbation data. Only data from within a radius of 20–40 km are considered. With this cross-section data, pressure perturbation wavelength is detected by the distance of local maxima or minima.

Figure 3c shows an example of the probability distribution of the wavelength of the pressure perturbation during hurricane landfall at 0100 UTC on 26 August 2017. Similar to the probability distribution of the wavelength of eddies, the probability distributions of the wavelengths of pressure perturbation from local maxima and minima are close to each other, with global maxima at around 0.5–1 km. The mean wavelength is 0.9 km. The similar mean wavelengths from eddies, rolls (Fig. 3a, b), and pressure perturbation (Fig. 3c) again confirm the relationship between pressure perturbation, rolls, and eddies. Once inflow convergence transports the rolls and creates strong rolls and eddies with strong wind shear near the eyewall,

the strong pressure perturbation can then transfer the eddy horizontal component (I_u) into the vertical component (I_w). Even after landfall, when strong rolls and eddies almost disappear as the wind shear weakens, the pressure perturbation can still transfer weak horizontal turbulence (I_u) into weak vertical turbulence (I_w), with a mean wavelength of about 0.9 km.

6 Summary

In this study, the one-way nested WRF-LES model simulation results from Li et al. (2021) are used to examine the structure and generation mechanism of rolls and associated coherent eddies in the hurricane boundary layer around Hurricane Harvey's landfall from 00 UTC 25 to 18 UTC 27 August 2017. The simulation results indicate that the aligned downstream rolls prevail throughout the entire hurricane boundary layer from near the surface to a height of 200–400 m. Extremely intense rolls with associated intense eddies occur at a height of 200–3000 m, within a radius of 20 to 40 km from the storm center.

During the simulation period, the vertical and horizontal components of the turbulence intensity of the intense coherent eddies, including rolls and other eddies, are related to the hurricane intensity. In other words, turbulence intensity increases with hurricane intensification. Before and during hurricane landfall, strong inflow convergence leads to horizontal advection of rolls throughout the entire hurricane boundary layer and combines with the strong wind shear there to generate the strong rolls and eddies near the eyewall with suitable thermodynamic (R_f at around -0.2 to 0.2) and dynamic conditions (strong negative inflow wind shear). After landfall, the decayed inflow weakens the inflow convergence and wind shear, leading to the quick reduction of strong rolls.

Once strong rolls and eddies occur near the eyewall, atmospheric pressure perturbation, which is caused by horizontal convergence, forces some TKE horizontal components (I_u) to turn into vertical components (I_w). The pressure perturbation force connects the rolls and eddies vertically with a similar wavelength of about 1 km. Meanwhile, the buoyancy term in the TKE equation is weak and negative; thus, it suppresses the vertical component of rolls and eddies. Therefore, under the necessary thermodynamic and dynamic conditions, the hurricane flow will generate strong rolls near the eyewall and then combine with air pressure perturbation to generate strong vertical turbulence motion near the eyewall of the hurricane. The simulated wavelength structure is similar to previous observations. More case studies will be conducted in future work.

Acknowledgements The authors would like to acknowledge high-performance computing support from Cheyenne (<https://doi.org/10.5065/D6RX99HX>) provided by NCAR's Computational and Information Systems Laboratory, sponsored by the National Science Foundation, and the computing resources of the Center for High-Performance Computing at the University of Utah. This study was supported by NSF Award # OAC-2004658 and NASA Award # 80NSSC20K0900 (ZP).

Author contributions XL and ZP both wrote the main manuscript text. XL prepared all figures. All authors reviewed the manuscript.

Declarations

Conflict of interest The authors declare no competing interests.

Open Access This article is licensed under a Creative Commons Attribution 4.0 International License, which permits use, sharing, adaptation, distribution and reproduction in any medium or format, as long as you give appropriate credit to the original author(s) and the source, provide a link to the Creative Commons licence,

and indicate if changes were made. The images or other third party material in this article are included in the article's Creative Commons licence, unless indicated otherwise in a credit line to the material. If material is not included in the article's Creative Commons licence and your intended use is not permitted by statutory regulation or exceeds the permitted use, you will need to obtain permission directly from the copyright holder. To view a copy of this licence, visit <http://creativecommons.org/licenses/by/4.0/>.

References

- Brown RA (1980) Longitudinal instabilities and secondary flows in the planetary boundary layer: a review. *Rev Geophys* 18(3):683–697. <https://doi.org/10.1029/RG018i003p00683>
- Ellis R, Businger S (2010) Helical circulations in the typhoon boundary layer. *J Geophys Res Atmos*. <https://doi.org/10.1029/2009JD011819>
- Ernst PA, Jisan MA, Ginis I (2019) On the characteristics of hurricane roll vortices over land. SURFO technical report no. 19-02, pp 16–27
- Etling D, Brown RA (1993) Roll vortices in the planetary boundary layer: a review. *Boundary-Layer Meteorol* 65(3):215–248
- Fernández-Cabán PL, Alford AA, Bell MJ, Biggerstaff MI, Carrie GD, Hirth B, Kosiba K, Phillips BM, Schroeder JL, Waugh SM, Williford E (2019) Observing Hurricane Harvey's eyewall at landfall. *Bull Am Meteorol Soc* 100(5):759–775. <https://doi.org/10.1175/BAMS-D-17-0237.1>
- Foster RC (2005) Why rolls are prevalent in the hurricane boundary layer. *J Atmos Sci* 62(8):2647–2661. <https://doi.org/10.1175/JAS3475.1>
- Fujita TT (1992) Damage survey of Hurricane Andrew in south Florida. *Storm Data* 34(8):176
- Gall R, Tuttle J, Hildebrand P (1998) Small-scale spiral bands observed in Hurricanes Andrew, Hugo, and Erin. *Mon Weather Rev* 126(7):1749–1766. [https://doi.org/10.1175/1520-0493\(1998\)126%3C1749:SSSBOI%3E2.0.CO;2](https://doi.org/10.1175/1520-0493(1998)126%3C1749:SSSBOI%3E2.0.CO;2)
- Gao K, Ginis I (2014) On the generation of roll vortices due to the inflection point instability of the hurricane boundary layer flow. *J Atmos Sci* 71(11):4292–4307. <https://doi.org/10.1175/JAS-D-13-0362.1>
- Gao K, Ginis I (2016) On the equilibrium-state roll vortices and their effects in the hurricane boundary layer. *J Atmos Sci* 73(3):1205–1222. <https://doi.org/10.1175/JAS-D-15-0089.1>
- Gao K, Ginis I (2018) On the characteristics of linear-phase roll vortices under a moving hurricane boundary layer. *J Atmos Sci* 75(8):2589–2598. <https://doi.org/10.1175/JAS-D-17-0363.1>
- Gao K, Ginis I, Doyle JD, Jin Y (2017) Effect of boundary layer roll vortices on the development of an axisymmetric tropical cyclone. *J Atmos Sci* 74(9):2737–2759. <https://doi.org/10.1175/JAS-D-16-0222.1>
- Guimond SR, Zhang JA, Sapp JW, Frasier SJ (2018) Coherent turbulence in the boundary layer of Hurricane Rita (2005) during an eyewall replacement cycle. *J Atmos Sci* 75(9):3071–3093. <https://doi.org/10.1175/JAS-D-17-0347.1>
- Heffter JL (1980) Transport layer depth calculations. In: *Bulletin of the American Meteorological Society*, vol 61, no 1. Amer Meteorological Soc, pp 97–97
- Hong SY (2010) A new stable boundary-layer mixing scheme and its impact on the simulated East Asian summer monsoon. *Q J R Meteorol Soc* 136(651):1481–1496. <https://doi.org/10.1002/qj.665>
- Hong SY, Pan HL (1996) Nonlocal boundary layer vertical diffusion in a medium-range forecast model. *Mon Weather Rev* 124(10):2322–2339. [https://doi.org/10.1175/1520-0493\(1996\)124%3C2322:NBLVDI%3E2.0.CO;2](https://doi.org/10.1175/1520-0493(1996)124%3C2322:NBLVDI%3E2.0.CO;2)
- Hong SY, Noh Y, Dudhia J (2006) A new vertical diffusion package with an explicit treatment of entrainment processes. *Mon Weather Rev* 134(9):2318–2341. <https://doi.org/10.1175/MWR3199.1>
- Huang L, Li X, Liu B, Zhang JA, Shen D, Zhang Z, Yu W (2018) Tropical cyclone boundary layer rolls in synthetic aperture radar imagery. *J Geophys Res Oceans* 123(4):2981–2996. <https://doi.org/10.1029/2018JC013755>
- Katsaros KB, Vachon PW, Black PG, Dodge PP, Uhlhorn EW (2000) Wind fields from SAR: Could they improve our understanding of storm dynamics? *Johns Hopkins APL Tech Dig* 21:86–93
- Katsaros KB, Vachon PW, Liu WT, Black PG (2002) Microwave remote sensing of tropical cyclones from space. *J Oceanogr* 58(1):137–151. <https://doi.org/10.1023/A:1015884903180>
- Keperth JD (1996) Comments on “The temperature of evaporating sea spray droplets.” *J Atmos Sci* 53(11):1634–1641
- LeMone MA (1973) The structure and dynamics of horizontal roll vortices in the planetary boundary layer. *J Atmos Sci* 30(6):1077–1091. [https://doi.org/10.1175/1520-0469\(1973\)030%3c1077:TSADOH%3e2.0.CO;2](https://doi.org/10.1175/1520-0469(1973)030%3c1077:TSADOH%3e2.0.CO;2)

- Li X, Pu Z (2021) Vertical eddy diffusivity parameterization based on a large eddy simulation and its impact on prediction of hurricane landfall. *Geophys Res Lett*, e2020GL090703
- Li X, Pu Z, Gao Z (2021) Effects of roll vortices on the evolution of Hurricane Harvey during landfall. *J Atmos Sci* 78(6):1847–1867. <https://doi.org/10.1175/JAS-D-20-0270.1>
- Lilly DK (1966) On the instability of Ekman boundary flow. *J Atmos Sci* 23(5):481–494. [https://doi.org/10.1175/1520-0469\(1966\)023%3C0481:OTIOEB%3E2.0.CO;2](https://doi.org/10.1175/1520-0469(1966)023%3C0481:OTIOEB%3E2.0.CO;2)
- Lorsolo S, Schroeder JL, Dodge P, Marks F Jr (2008) An observational study of hurricane boundary layer small-scale coherent structures. *Mon Weather Rev* 136(8):2871–2893. <https://doi.org/10.1175/2008MWR2273.1>
- Makin VK (1998) Air-sea exchange of heat in the presence of wind waves and spray. *J Geophys Res Oceans* 103(C1):1137–1152. <https://doi.org/10.1029/97JC02908>
- Morrison I, Businger S, Marks F, Dodge P, Businger JA (2005) An observational case for the prevalence of roll vortices in the hurricane boundary layer. *J Atmos Sci* 62(8):2662–2673. <https://doi.org/10.1175/JAS3508.1>
- Mourad PD, Walter BA (1996) Viewing a cold air outbreak using satellite-based synthetic aperture radar and advanced very high resolution radiometer imagery. *J Geophys Res Oceans* 101(C7):16391–16400. <https://doi.org/10.1029/96JC01123>
- Nakanishi M, Niino H (2012) Large-eddy simulation of roll vortices in a hurricane boundary layer. *J Atmos Sci* 69(12):3558–3575. <https://doi.org/10.1175/JAS-D-11-0237.1>
- Nolan DS (2005) Instabilities in hurricane-like boundary layers. *Dyn Atmos Oceans* 40(3):209–236. <https://doi.org/10.1016/j.dynatmoce.2005.03.002>
- Saffir HS (1973) Hurricane wind and storm surge. *Mil Eng* 65(423):4–5
- Skamarock WC, Klemp JB, Dudhia J, Gill DO, Liu Z, Berner J, Wang W, Powers JG, Duda MG, Barker DM, Huang XY (2019) A description of the advanced research WRF model version 4. National Center for Atmospheric Research: Boulder, p 145
- Wakimoto RM, Black PG (1994) Damage survey of Hurricane Andrew and its relationship to the eyewall. *Bull Am Meteorol Soc* 75(2):189–202. [https://doi.org/10.1175/1520-0477\(1994\)075%3C0189:DSOHA%3E2.0.CO;2](https://doi.org/10.1175/1520-0477(1994)075%3C0189:DSOHA%3E2.0.CO;2)
- Wang S, Jiang Q (2017) Impact of vertical wind shear on roll structure in idealized hurricane boundary layers. *Atmos Chem Phys* 17(5):3507–3524. <https://doi.org/10.5194/acp-17-3507-2017>
- Weckwerth TM, Wilson JW, Wakimoto RM, Crook NA (1997) Horizontal convective rolls: Determining the environmental conditions supporting their existence and characteristics. *Mon Weather Rev* 125(4):505–526. [https://doi.org/10.1175/1520-0493\(1997\)125%3C0505:HCRDTE%3E2.0.CO;2](https://doi.org/10.1175/1520-0493(1997)125%3C0505:HCRDTE%3E2.0.CO;2)
- Wurman J, Kosiba K (2018) The role of small-scale vortices in enhancing surface winds and damage in Hurricane Harvey (2017). *Mon Weather Rev* 146(3):713–722. <https://doi.org/10.1175/MWR-D-17-0327.1>
- Wurman J, Winslow J (1998) Intense sub-kilometer-scale boundary layer rolls observed in Hurricane Fran. *Fran Sci* 280(5363):555–557. <https://doi.org/10.1126/science.280.5363.555>
- Young GS, Kristovich DA, Hjelmfelt MR, Foster RC (2002) Supplement to rolls, streets, waves, and more. *Bull Am Meteorol Soc* 83(7):1001–1001. [https://doi.org/10.1175/1520-0477\(2002\)083%3C0997:RSWAMA%3E2.3.CO;2](https://doi.org/10.1175/1520-0477(2002)083%3C0997:RSWAMA%3E2.3.CO;2)
- Zhang JA, Drennan WM (2012) An observational study of vertical eddy diffusivity in the hurricane boundary layer. *J Atmos Sci* 69(11):3223–3236. <https://doi.org/10.1175/JAS-D-11-0348.1>
- Zhang JA, Katsaros KB, Black PG, Lehner S, French JR, Drennan WM (2008) Effects of roll vortices on turbulent fluxes in the hurricane boundary layer. *Boundary-Layer Meteorol* 128(2):173–189. <https://doi.org/10.1007/s10546-008-9281-2>
- Zhao Z, Chan PW, Wu N, Zhang JA, Hon KK (2020) Aircraft observations of turbulence characteristics in the tropical cyclone boundary layer. *Boundary-Layer Meteorol* 174(3):493–511. <https://doi.org/10.1007/s10546-019-00487-8>
- Zhou B, Sun S, Sun J, Zhu K (2019) The universality of the normalized vertical velocity variance in contrast to the horizontal velocity variance in the convective boundary layer. *J Atmos Sci* 76(5):1437–1456. <https://doi.org/10.1175/JAS-D-18-0325.1>
- Zhu P (2008a) A multiple scale modeling system for coastal hurricane wind damage mitigation. *Nat Hazards* 47(3):577–591. <https://doi.org/10.1007/s11069-008-9240-8>
- Zhu P (2008b) Simulation and parameterization of the turbulent transport in the hurricane boundary layer by large eddies. *J Geophys Res Atmos*. <https://doi.org/10.1029/2007JD009643>
- Zhu P, Wang Y, Chen S, Curcic M, Gao C (2016) Impact of storm-induced cooling of sea surface temperature on large turbulent eddies and vertical turbulent transport in the atmospheric boundary layer of Hurricane Isaac. *J Geophys Res Ocean* 121(1):861–876. <https://doi.org/10.1002/2015JC011320>

Publisher's Note Springer Nature remains neutral with regard to jurisdictional claims in published maps and institutional affiliations.